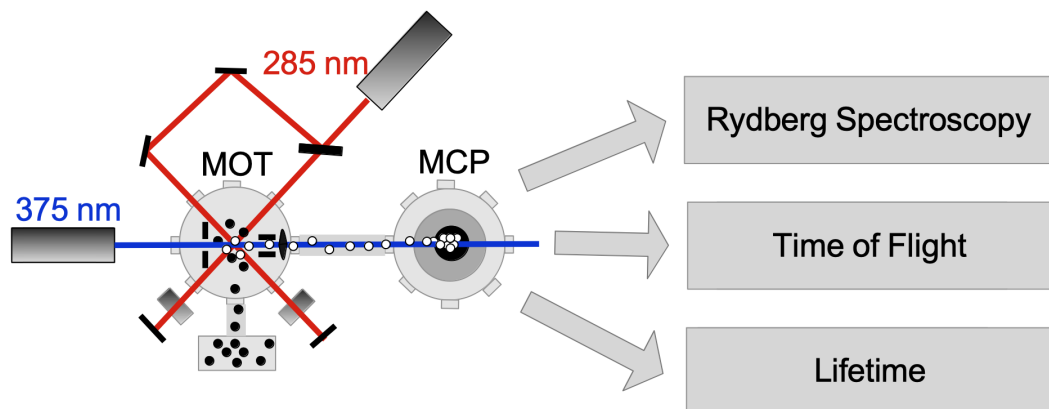


Detection of Rydberg Mg Atoms by Pulsed Field Ionization

Semester Thesis

Lara Ostertag

January 2022



Under the kind guidance of
Dr. Henry Fernandes Passagem
and
Prof. Dr. Jonathan Home

Trapped Ion Information Group

ETH zürich

Contents

1	Abstract	i
2	Introduction	1
2.1	Rydberg Atoms	1
2.1.1	Advantages of Rydberg Atoms	1
2.2	Motivation	2
2.3	Outline	3
3	Experimental Setup	4
3.1	Lasers	5
3.2	MOT Description	6
4	Experimental Measurements	9
4.1	Ionization Electric Field	10
4.2	Experimental Time Sequence	11
4.3	Rydberg Atom Spectroscopy	12
4.3.1	Quantum Defect Theory	12
4.3.2	Addressing Rydberg States Using a MCP	13
4.4	Time of Flight Measurements	14
4.5	Lifetime Measurements	16
5	Conclusion and Outlook	18
6	Acknowledgements	19
A	Appendix	23
A.1	Calculated Transition Frequencies and Wavelengths	23
A.2	Lifetime of different Rydberg states	24

1 Abstract

Exciting the outer electron of a neutral atom (in this case Mg) to a high principle number n state, creates a neutral Rydberg atom, where the Rydberg electron is further removed from the atom core. By exciting the Rydberg electron to a circular state of maximum angular momentum l , this causes a minimum overlap of the electron and the core wavefunction. Ideally, this property can be used to encode quantum information in the Rydberg atom, by creating qubit (quantum bit) states for different energy levels. Furthermore, due to the distant outer electron, the neutral Rydberg atom core can be treated similarly to a slightly positive ion.

In efforts to achieve this, it is necessary to detect, as well as selectively address different Rydberg states. This was achieved using pulsed field ionization. The Magnesium Rydberg atoms described in this thesis are generated using two-photon excitation. In other words, a 285 nm laser excites the electron from the $3s^2 \ ^1S_0$ (ground state) to the $3s \ 3p \ ^1P_1$ state. Next, a 375 nm excites the same electron to either the $3s \ ns \ ^1S_0$ or $3s \ nd \ ^1D_2$ state, as determined by selection rules. The Rydberg atoms are prepared in a magneto-optical trap (MOT), ionized by an electric field pulse and detected using a micro-channel plate (MCP). This made it possible to selectively detect Rydberg states. Using quantum defect theory, the experimentally found states were assigned to their specific states. Furthermore, flight time measurements were performed in efforts to achieve selective ionization detection and lifetimes of different states were measured.

2 Introduction

2.1 Rydberg Atoms

Rydberg atoms are atoms where the outermost electron (or sometimes multiple electrons) are excited to a very high principal quantum number n . While there is no exact number of what quantifies a "high" quantum number, a principal number of 100 or higher can definitely be considered such. The excitation of the outer electron causes it to be further removed from the nucleus. Consequentially, Rydberg atoms can be treated similar to Hydrogen atoms, since they can be modeled by one outer electron surrounding a positively charged core. Quantum defect theory (as explained in section 4.3.1) accounts for the corrections that need to be considered when approximating a Rydberg atom as a Hydrogen atom.

Rydberg atoms get their name from the Swedish physicist Johannes Rydberg, who found a relationship between the wavelength of an emitted photon and the different spectral lines in Hydrogen:

$$\frac{1}{\lambda} = R_H \left(\frac{1}{n_1^2} - \frac{1}{n_2^2} \right)$$

where R_H corresponds to the Rydberg constant ($1.097 * 10^7 m^{-1}$) and n_1 and n_2 are integers where $n_2 > n_1$ (1). These integers were later named principal quantum numbers and relate to the fact that the energy levels in an atom are quantized.

2.1.1 Advantages of Rydberg Atoms

There are five main qualities that make Rydberg atoms very promising for quantum computing.

Firstly, Rydberg atoms have a relatively large size. This can be better understood using Bohr's model. The centripetal acceleration of the electron in Rydberg state equals the Coulomb force experienced by the electron. Taking into account Bohr's quantization of angular momentum $m_e v r = n \hbar$ (m_e equals the mass of the electron), one can solve for the electron radius r :

$$\frac{m v^2}{r} = \frac{e^2}{4\pi\epsilon_0 r^2} \quad \Rightarrow \quad r = \frac{4\pi\epsilon_0 \hbar^2}{e^2 m} n^2 = a_0 n^2$$

where a_0 is the Bohr radius. Consequentially, the electron radius scales proportional to n^2 , making Rydberg atoms almost macroscopic in size. This is very useful since single atom addressing, which is crucial for single qubit control, becomes a lot easier.

Secondly, Rydberg atoms have strong dipole properties and therefore strong electro-static interactions, since the outer electron is further removed from the nucleus. Their interactions can range to a scale of 10-100 microns (1), which

make them particularly interesting for quantum entanglement. These interactions are important in quantum computing, since they enable quick quantum gate operations.

Thirdly, Rydberg atoms have a strong atomic polarizability, which scales as n^7 where n is the principal quantum number (2).

Fourthly, while significant improvements are still required to further increase the lifetime of Rydberg atoms, their relatively long lifetime ((at around 100 μ s) is very promising (1). This is further explained in chapter A.2. In a nutshell, as the orbital angular momentum l increases, the overlap of the electron and core wavefunctions decreases.

Fifthly, Rydberg atoms are made from neutral atoms. As a consequence, when the outer electron is not excited to Rydberg state, the atom does not strongly interact with its environment and avoids strong decoherence. While black-body radiation strongly limits the lifetime of Rydberg atoms and causes decoherence, it is possible to switch between Rydberg states, when performing a gate, and then turning off the interaction with the environment through Stark shifting or by de-exciting the Rydberg electron (1).

2.2 Motivation

As shown in section 2.1.1, there are multiple properties that make Rydberg atoms so promising for quantum computing and simulation. However, two challenges also have to be considered. Firstly, atomic motion causes qubit instability and secondly, Rydberg state lifetimes, which lie at around 100-200 μ s at room temperature, are not sufficiently long, compared to the currently achievable gate time operation speed (3).

However, the recent paper by Cohen and Thompson (3) shows extremely promising results to prevent errors from atomic motion using dynamical decoupling sequences and create long-lived circular Rydberg states. This can be achieved by creating circular Rydberg states, meaning states with a large principal number n , as well a maximum angular and magnetic quantum numbers l and m , where $l=|m|=n-1$. These states have extremely long lifetimes at around 10 ms at cryogenic temperatures. Their long life times are due to the fact that radiative decay can only occur to the next-highest circular state and this transition lies in the microwave-frequency regime. Furthermore, lifetimes can be increased to up to 100 seconds, by suppressing local density of states at the single transition frequency that causes decay. These are extremely promising results, since they suggest an improvement of up to six orders of magnitude compared to the lifetime of low- l states (3)!

Since circular Rydberg states are very hard to produce, due to their large angular momentum difference of around 50, a drastic increase in lifetime does not

necessarily translate to a drastic increase in fidelity. However, using multiple circular Rydberg states to encode qubits is a promising method to sidestep this issue, making it possible to get two-qubit gate errors of around 10^{-5} using 100 circular Rydberg atoms (3).

These promising predictions strongly motivate the usage of circularized Rydberg states. As a first step to achieving these states, it is necessary to be able to individually address different Rydberg states. Consequentially, this project consists of using pulsed field ionization to detect Rydberg states with high spectroscopic resolution using a micro-channel plate.

2.3 Outline

This semester thesis is structured as follows:

Having given a brief introduction to what Rydberg atoms are and why they are interesting to use for quantum computation in section 2.1, chapter 3 continues by outlining the experimental setup used to generate and detect Rydberg atoms. This section also includes some further detail about what the MOT and MCP are and how they are used for trapping and detection.

The main experimental results can be divided into three categories: Mg spectroscopy using MCP in section 4.3, time of flight measurements in section 4.4 and lifetime measurements in section 4.5. The Mg spectroscopy section shows a frequency sweep of the Rydberg excitation laser, making it possible to find resonant transitions and therefore, find different Rydberg states using time delayed field ionization and detection on an MCP. Using results obtained by quantum defect theory (section 4.3.1), it is possible to calculate expected transition frequencies and thereby assign Rydberg states to the measured transitions. Being able to address particular Rydberg states makes it possible to perform time of flight measurements of these states. Since Rydberg states are highly sensitive to small changes in electric fields, slowly increasing the ionization electric field makes it possible to differentiate different Rydberg states based on their difference in time of flight. Lastly, by varying the time delay between the Rydberg excitation pulse and the ionization pulse, it is possible to measure the number of Rydberg atoms for different time delays, from which the lifetime can be extracted. These results are then summarized in chapter 5, which also provides an outlook.

3 Experimental Setup

The following experiments were performed in a Magnesium MOT. The experimental procedure when producing Mg Rydberg atoms can be broken up into the following steps:

1. Mg Sublimation:

The oven heats solid Mg and the gaseous atoms are trapped by the MOT. While ^{25}Mg and ^{26}Mg isotopes are also present, the experiment uses the most abundant one, ^{24}Mg , which has a natural abundance of 79.0% (4).

2. State Excitation:

The electron configuration of the Mg atom at its ground state is $1s^2 2s^2 2p^6 3s^2 {}^1S_0$, which in the following will be referred to as $3s^2 {}^1S_0$. In order to excite the valence electron to a Rydberg state, a two-photon excitation mechanism is used.

(a) 285 nm laser:

Using MOT beams (as can be seen in figure 4), which consist of 285 nm diode lasers, the valence electron is excited from the $3s^2 {}^1S_0$ to the $3s3p {}^1P_1$ state. This can be seen by the red arrow in figure 1. The frequency of the Mg MOT transition is at 1050.8105 THz (285.2964 nm) (5). In order to keep atoms trapped in the MOT, the laser is locked to a molecular iodine vapor cell, which has a transition line at twice the laser frequency, namely 570 nm (6). How a laser beam of this wavelength is created can be seen in more detail in section 3.1.

(b) 375 nm laser:

Next, a tunable 375nm external cavity diode laser (ECDL) is used to address different Rydberg states. According to dipole selection rules ($l'=l\pm 1$), a transition will only occur to states that have an angular momentum of $l=0$ or 2, which correspond to the s and d state respectively. These transitions to high n Rydberg states are marked by a blue arrow in figure 1 and can be written down as follows: $3s3p {}^1P_1 \Rightarrow 3snd {}^1D_2$ and $3s3p {}^1P_1 \Rightarrow 3sns {}^1S_0$.

3. Fluorescence Measurement:

The excitation to the $3s3p {}^1P_1$ is a luminous transition, meaning that a UV sensitive camera can be used to detect the 285 nm photons that are being emitted. This can be seen by the blue intensity curve, as well as the image surrounded in blue in figure 2.

Once the atoms are excited to Rydberg state, they are no longer visible in the UV sensitive camera, meaning that a resonance is found when there is a drop in MOT fluorescence as can be seen in figure 3.

4. Field Ionization:

Next, field ionization electrodes in the MOT (indicated by the green marks

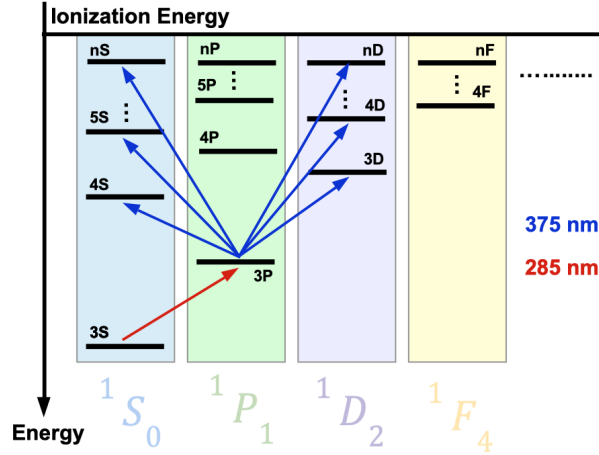


Figure 1: Energy Level diagram for singlet states in Mg, depicting two-photon excitation to Rydberg states (not to scale).

in figure 4) ionize the Rydberg atoms in the MOT chamber. Using deflectors and an electrostatic lens, the ionized Rydberg atoms are guided to the micro-channel plate (MCP) chamber.

5. MCP Detection: The MCP chamber contains high voltage electrodes. The electrode below the incoming Rydberg atoms has a strong negative voltage, which causes the ions to move upwards, towards the MCP. As the ions hit the MCP, they rip off electrons from the MCP surface. This causes a cascade effect, which results in a voltage and therefore an electrical signal that can be measured on an oscilloscope (1).

The entire setup can be seen in figure 4. Three perpendicular 285 nm laser beams are applied to trap the atoms. The third beam entering from the top of the MOT cannot be seen in this figure, but can instead be seen in figure 6.

3.1 Lasers

Figure 5 shows a simplified depiction of how 245 nm laser light is created. An infrared (IR) diode laser of wavelength 1140 nm with a power of 50-100 mW is used. A tapered amplifier (TA) then increases the power from the single mode laser to 700 mW. The laser light gets fed into a bow-tie cavity containing a lithium triborate (LBO) non-linear crystal. Here the frequency is doubled, producing 570 nm green light. Part of this light is deflected to the molecular iodine cell using a beam splitter, where the laser frequency is locked to the 570 nm absorption line. The remaining light passes through a second nonlinear crystal, where the frequency is doubled to the intended wavelength of 245 nm. The final power lies around 1 mW per beam.

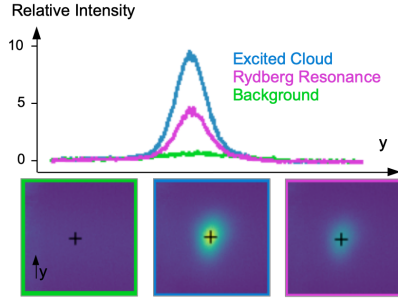


Figure 2: Comparison of relative intensity of fluorescent Mg cloud (excited by 285 nm laser) and fluorescence drop due to Rydberg resonance

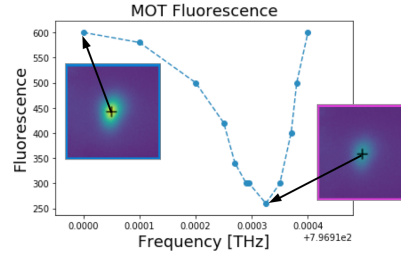


Figure 3: Loss in fluorescence due to resonant transition with 375 nm laser exciting a valence electron to Rydberg state as a function of frequency

Meanwhile, the 375 nm laser (with a power of around 5.5 mW close to the MOT) is able to excite the Rydberg electron from principal number 50 to 110, which corresponds to a frequency range of about 1.13 THz. In order to find a frequency resonance of a Rydberg state, the diode laser is initially not locked. The laser controller is used to find the resonance, which can be found by the fluorescence drop, as seen in the pink image in figure 2. A script then reads off the MCP signal and uses a proportional integral derivative (PID) control loop to keep the laser locked to a certain set point. The laser frequency can then be fine-tuned by maximizing the MCP count.

3.2 MOT Description

A magneto-optical trap (MOT) is used to trap and cool neutral Mg atoms. This process is performed using three intersecting mutually orthogonal, circularly-polarized, red-detuned laser beams (visible in figure 6), in combination with a weak quadruple magnetic field (visible in figure 7).

The choice of setup can be understood by answering the following questions:

1. How can a laser move an atom?

Laser light shining on an atom can be modeled as a two level system that is bombarded with a stream of photons with velocity v . Due to momentum conservation, when a photon (with momentum $\hbar k$) is absorbed, the atom is excited and has a momentum kick $mv = \hbar k$ in the direction of travel of the photon. After a certain time, spontaneous emission occurs and the atom moves back to the ground state. Since spontaneous emission is isotropic, the recoil is in a random direction and averages out, leaving the net momentum gain of the atom after n cycles to be at $Mv = n\hbar k$. Therefore, the change in momentum creates a force in the direction of

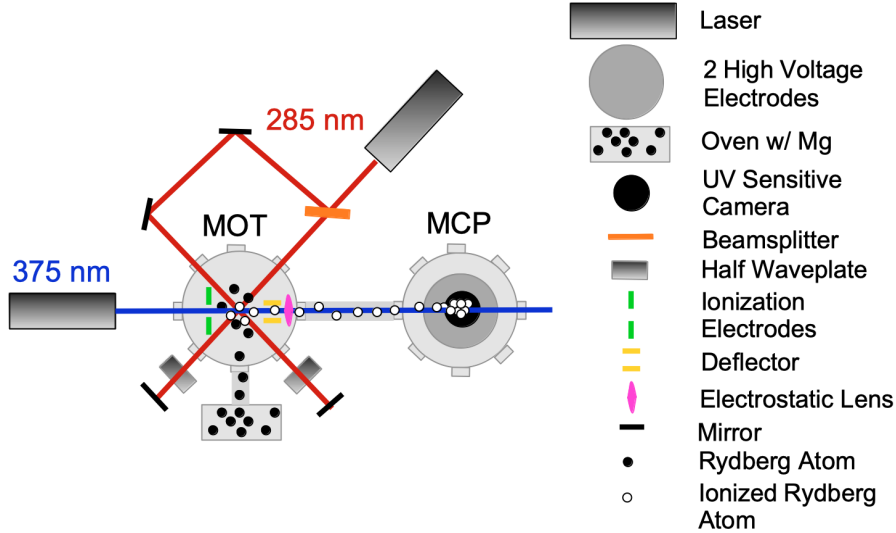


Figure 4: Top view of the experimental setup showing the MOT and MCP chamber with a 285 nm and 375 nm laser (not to scale). A third beam coming from the 285 nm laser passes through the MOT from the top and cannot be seen in the image.

travel of the photons.

2. How does the force become position dependent and why are the lasers red detuned?

An atom propagating in the opposite direction of a laser beam (kv_0) with frequency w_L sees a Doppler shifted frequency of $w_L - kv$. If the laser beam is red detuned in such a way that $w_L = \frac{w_o}{1+v/c}$ where w_o is the resonance frequency, the atom will see a frequency that is Doppler shifted to the resonance frequency, thereby causing a photon to be absorbed and the atom to slow down. If the atom were to move in the same direction as the laser beam, it would see a frequency even further detuned from resonance, causing it not to be slowed down and continue to move in the same direction.

3. Why are the laser beams polarized in a certain direction and what role does the B-field play?

The two anti-Helmholtz coils generate a magnetic quadrupole field (as shown in figure 7) and are placed in such a way that the point of no magnetic field coincides with the overlapping region of the three laser beams. Hence, the atoms in the atomic vapor experience a restoring force towards the center of the trap. This B field leads to the Zeeman effect, where the sublevels get shifted by an energy proportional to the B field and the degeneracy of the hyperfine levels gets lifted. By using circularly polar-

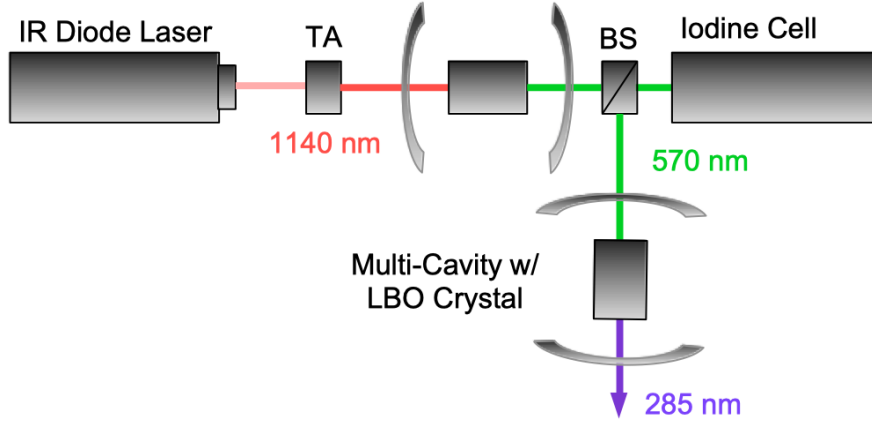


Figure 5: Simplified setup showing how 275 nm laser light is created using an infrared diode laser, a tapered amplifier (TA), multi-cavities containing LBO crystals, a beam splitter (BS) and laser locking using an iodine cell. Not to scale.

ized light, it is possible to have selective absorption for certain states. In other words, the σ^+ circularly polarized beam causes a transition with $\delta m_F = +1$ and the σ^- circularly polarized beam causes a transition with $\delta m_F = -1$. If one now has two beams with opposite polarization facing one another, this causes a magnetic field gradient and the sublevel splitting changes along the axes of the laser beams (as seen in figure 8). Consequentially, when the atoms are located closer to the σ^+ polarized light, the atoms see a frequency from the σ^+ that is close to the atomic resonance, causing atoms to experience a net force in the direction of the σ^+ polarized beam. Meanwhile, the σ^- polarized beam is too far detuned to have a significant effect. The opposite case occurs when the atoms are located closer to the σ^- beam, causing a net movement in the direction of the σ^- beam. This leads to an overall movement of the atoms to the center of the trap caused by the counter-propagating oppositely detuned beams (as seen in figure 6).

Further information on how laser cooling and trapping of neutral atoms can be achieved using a MOT can be found in the paper by Kłowski et al (7).

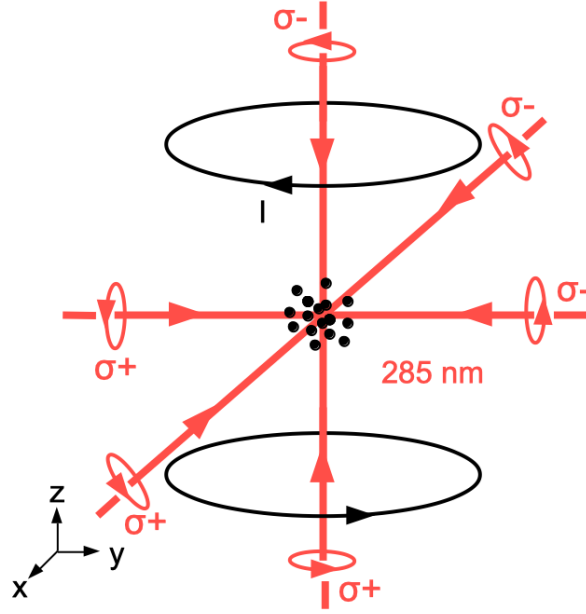


Figure 6: Side View inside the MOT, showing three mutually orthogonal, counter-propagating, polarized, red detuned 285 nm laser beams that enable trapping of neutral atoms. Modified figure from Kowalski et al. (7)

4 Experimental Measurements

In efforts to accurately detect different Rydberg states and successfully create circularly polarized states, as well as measure their lifetime, the following three experiments were performed: 1) spectroscopy of Rydberg atoms using an MCP (section 4.3.2), 2) time of flight measurements (section 4) and 3) lifetime measurements (section A.2).

The experimental time sequence for these experiments can be seen in section 4.2. The experiments make use of selective ionization detection, which is a promising method to be able to measure the spectrum of Mg Rydberg atoms. An ionization field (applied with a time delay) is used to ionize Rydberg atoms (as explained in section 4.1). By using an RC circuit, this field increases slowly, causing different states to ionize at different times. By measuring the time of flight, meaning the time it takes for the ionized Rydberg atom to reach the MCP, the exact state of the atom can be deduced. This method promises to be able to identify different l and m quantum states, which is further explained in section 4.

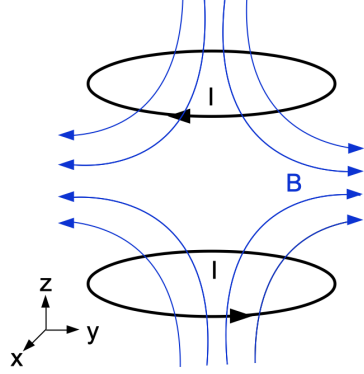


Figure 7: Anti-Helmholtz coils leading to a magnetic quadrupole field

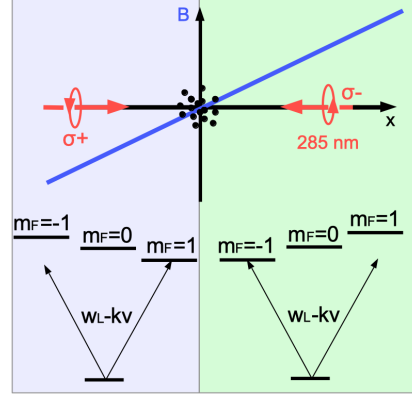


Figure 8: B field along the axis of two counter-propagating beams with opposite polarization, with the Zeeman shifted sublevels and Doppler shifted frequencies causing an atomic resonance transition shown below. Modified figure from Kowalski et al.

4.1 Ionization Electric Field

Time of flight measurements rely on the principle that different Rydberg states require different ionization electric fields. Unlike ground state electrons, Rydberg atoms are highly sensitive to external electric fields. Hence, one has to consider the combined Coulomb-Stark potential

$$V = -\frac{1}{r} + Ez$$

which is given for an electric field E applied along the z direction and a Rydberg electron orbit with radius r (in atomic units). Equating the derivative of the potential to zero gives a saddle point location at $z = -\frac{1}{\sqrt{E}}$ for a potential of $V = -2\sqrt{E}$. For states with magnetic quantum number $m=0$ no additional centrifugal potential is needed. Therefore, the ionization electric field is given by $E = \frac{W^2}{4}$, where W is the binding energy of the electron (2). W can be calculated using the kinetic and potential energies of the electron, which gives $\frac{1}{2r}$.

Combining the ionization electric field with the binding energy and the Rydberg radius, which was found in chapter 2.1, leads to the following ionization electric field for a Rydberg atom:

$$E = \frac{W^2}{4} = \frac{\left(\frac{-1}{2r}\right)^2}{4} = \frac{1}{16n^{*4}}$$

However, instead of using the principal quantum number n , we will use the effective principal number $n - \delta_{n,l}$ as described in section 4.3.1 (1).

While this calculation is a good classical approximation that is sufficient for the following calculations, it is important to note that it only works for $m=0$ states and ignores the Stark shift. Atoms of different energy levels can mix with one another as the ionization electric field increases, causing them to move to a different energy level. This potentially leads to a broadening in the ionization energy and an ionization threshold of $E = \frac{1}{9n^{*4}}$ instead (8).

4.2 Experimental Time Sequence

The following experiments all use the time sequence shown in figure 9. The MOT beams (shown in red in figure 6) are initially turned on, confining the Mg atom cloud at the center of the MOT and exciting the valence electron to the $3p \ ^1P_1$ state. After 5 seconds, the 375 nm laser is turned on for 5 ms, after which both the MOT beams and the 375 nm laser are turned off. Depending on the exact wavelength of the tunable 375 nm laser, the atoms will be in a certain Rydberg state. After a certain time delay τ , the ionization field is turned on. An RC circuit is used to slowly increase the ionization field, which is necessary for the time of flight measurements, as explained in section 4. After $23 \mu s$ the ion signal is measured for $2 \mu s$ using the MCP. A few μs after that, the ionization field is also turned off.

For the spectroscopy of Rydberg states and time of flight measurements, the time delay τ is held constant at $1.4 \mu s$. Meanwhile, for lifetime measurements, the time delay is varied, in order to measure the ion signal for different time delays. From the exponential decay of the ion signals, the lifetime for different Rydberg states can be derived.

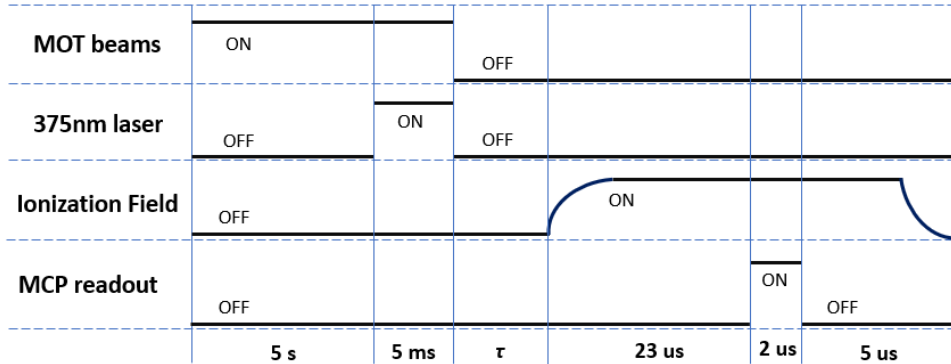


Figure 9: Time Sequence used for experiments, where the time delay τ is held constant (at $1.4 \mu s$) for the spectroscopy of Rydberg states and time of flight measurements. For lifetime measurements, one varies the time delay τ .

4.3 Rydberg Atom Spectroscopy

4.3.1 Quantum Defect Theory

Quantum defect theory is a multi-channel scattering approach, where the quantum defect can be seen as a correction to the hydrogen Coulomb potential, in order to find energy eigenstates of non-hydrogen atoms (9).

Instead of using the equation $E = -\frac{13.6}{n^2}eV$ (used for finding the energy in a hydrogen atom), one can use the Rydberg-Ritz formula to determine the energy level of a singlet Magnesium atom (10).

$$E(n, l, j) = \frac{-R_{Mg}}{n^{*2}} = \frac{-R_{Mg}}{(n - \delta_{n,l,j})^2}$$

where

$$\delta_{n,l,j} = E_{l,j} + \frac{A_{l,j}}{(n - E_{l,j})^2} + \frac{B_{l,j}}{(n - E_{l,j})^4} + \frac{C_{l,j}}{(n - E_{l,j})^6} + \dots$$

Here n^* stands for the effective principal quantum number, while $E_{l,j}$, $A_{l,j}$, $B_{l,j}$ and $C_{l,j}$ stand for the quantum-defect Rydberg-Ritz expansion coefficients. The Rydberg constant for Mg I equals $109734.83884 \text{ cm}^{-1}$ (10). Since the following calculations concentrate on resolving different principal numbers n , for the moment the angular momentum subscript j is neglected.

Comparing the predicted energy levels for different expansion coefficients from different sources (10; 11; 12) with experimental data, showed that the values given by Dyubko et al. (10) most accurately predict the experimental data. Therefore, the following calculations use the expansion coefficients seen in table 1, which are valid for $5 \leq n \leq 39$. While not applicable for higher n states, extrapolation is still possible. By collecting more resonance frequencies, it will be possible to find an even better fit to the measurements by adjusting the quantum defect parameters further.

Since the calculated energy values are energy differences from the ionization energy, one should subtract them from the ionization energy of Mg 1. According to the NIST database, this value equals $61,671.05 \text{ cm}^{-1}$ (5; 13).

Table 1: Quantum Defect Rydberg-Ritz Expansion Coefficients for Mg I (10)

State	E_l	A_l	B_l	C_l
1S_0	1.525367	-0.0310	1.364	-3.37
1P_1	1.051333	-0.3679	0.874	-3.51
1D_2	0.612110	-3.147	8.25	-5.54

Lastly, by subtracting the energy of the $3s3p \ ^1P_1$ state of Mg I ($35,051.264 \text{ cm}^{-1}$ (13)) from the calculated energy of a certain Rydberg state, one can calculate the required frequency to create a certain Rydberg state.

4.3.2 Addressing Rydberg States Using a MCP

In order to use neutral Rydberg atoms to encode quantum information, it is necessary to unambiguously address specific Rydberg states. Therefore, it is crucial to create an accurate spectrum of different Rydberg states, as well as assign the resonance frequencies to specific principal numbers n . This can be done using quantum defect theory (as shown in section 4.3.1). Previously, the Trapped Ion Quantum Information group performed spectroscopy of Mg by measuring the relative extinction rate of Rydberg atoms in a magneto-optical trap as detected by a UV sensitive camera (6). In the following experiments, Mg spectroscopy is performed using electric field ionization and detected using an MCP detector. This not only shows that an alternative method for Rydberg atom detection is possible, but also provides a direct method of detection. Initially, Rydberg atoms are still detected through a lack of fluorescence (see figure 3). For more accurate determination of frequency, the MCP directly measures the electrical signal produced by the ionized Rydberg atoms.

The previously mentioned two-step laser excitation process (section 3) makes it possible to perform a spectroscopy of Mg Rydberg atoms (as well as then individually address certain Rydberg states). The Rydberg atoms are therefore in the $3snd\ ^1S_0$ or $3snd\ ^1D_2$ state. Using a PID protocol makes it possible to keep the 375 nm laser locked to resonance frequency stable. By scanning the frequency on a frequency window of around 0.5 GHz and measuring the MCP counts, one can determine the precise resonance frequency of different states. It is advantageous to use a step size of at least 25 MHz.

This frequency sweeping can be seen in figure 10, which shows the spectra of two different frequency ranges. A Gaussian fit

$$G = H + Ae^{-\frac{(x-\mu)^2}{2\sigma^2}}$$

determines the peak MCP count and thereby the precise resonance frequency. In the case of figure 10, the resonance frequencies were found to be at 796.8678 THz and 796.9105 THz.

The Gaussian fit (shown in figure 10) can also be used to get information about the signal quality. For instance, looking at the frequency scan around the resonance frequency found at 796.9105 THz, one can find that the background noise H lies at 3.21 counts. Meanwhile, the standard deviation σ lies at 19 MHz.

After performing frequency scans and finding the precise resonance frequency using Gaussian fits, one can use the theoretical resonance frequencies shown in table A.1 (which were calculated using quantum defect theory as described in section 4.3.1) to assign experimentally measured resonances to certain Rydberg states. The agreement of experimentally found resonance frequencies and calculated ones is shown in table 2 and figure 11. The difference between measured and calculated frequency is relatively high at around 0.0126 THz for states with

4.4 Time of Flight Measurements 4 EXPERIMENTAL MEASUREMENTS

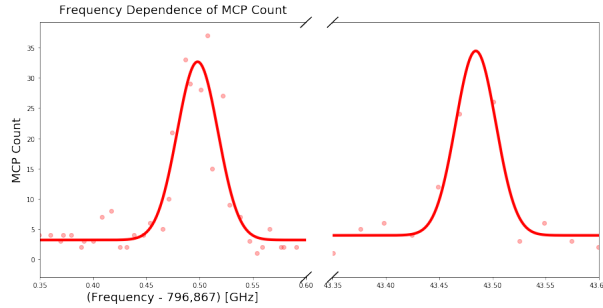


Figure 10: Scanning the resonance frequency of the 375 nm laser for two different frequency ranges and measuring MCP count, finding the 54D and 55D states and their resonance frequencies

principal numbers between 50 and 60. Meanwhile, the difference for states with principal numbers between 100 and 120 lies at around 781 MHz. This can partially be explained by the fact that the frequency spacing for different principal numbers decreases with increasing frequency.

Table 2: Experimentally Measured Resonances

Measured Frequency [THz]	Calculated Frequency [THz]	Associated principal number
796.8678	796.886959	54
796.9105	796.929008	55
797.0067	797.006494	57
797.7077	797.708068	100
797.7145	797.714670	101
797.7962	797.794394	117

4.4 Time of Flight Measurements

Being able to individually address different Rydberg states makes it possible to measure and compare time of flight data. The experiment uses the time sequence shown in figure 9. As explained in section 4.1, Rydberg atoms are highly sensitive to external electric fields and different Rydberg states require different ionization electric fields. For instance, the ionization electric fields for principal numbers n of 54, 55 and 57 lie at 39.540 V/cm, 36.711 V/cm and 31.774 V/cm respectively.

These values were found using the equation $E = \frac{1}{16n^{*4}}$ found in section 4.1, where n^* corresponds to the effective principal number $n - \delta_{n,l}$. $\delta_{n,l}$ can be calculated given the quantum defect Rydberg-Ritz expansion coefficients given in table 1. The resultant ionization electric field was then converted from atomic

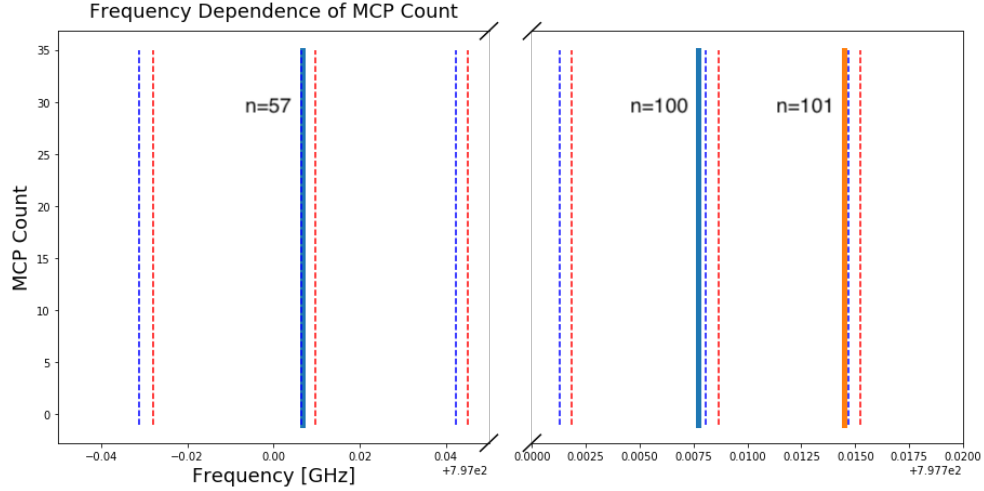


Figure 11: This graph shows a comparison between measured (solid lines) and calculated (dotted lines) resonance frequencies for two different frequency ranges

units to SI units.

Consequentially, higher Rydberg states require a smaller ionization electric field. If one now uses an RC circuit, the voltage that ionizes the atom increases slowly, meaning that a higher ionization voltage will be reached at a later time. This causes lower Rydberg states to have a longer time of flight, making it possible to distinguish different Rydberg states from one another based on their difference in time of flight.

Figure 12 shows such a measurement. The 375nm laser was tuned to selectively address certain Rydberg states and the time of flight can be extracted by looking at the ion signal peak at a certain time. The data shows the time of flight for principal numbers 54 (shown in blue and orange), 55 (shown in green and red) and 57 (shown in purple and brown). The measurements were performed using an RC circuit with a resistance of 1 k Ω and a capacitance of 2.2 nF. Unfortunately, no clear difference in time of flight can be seen, since all time values lie at around 24 μ s. This is likely due to the fact that the ionization voltage increases very suddenly, meaning that the ionization voltage between different states is reached at time intervals that are too small to clearly identify. Therefore, the next step would be to include an RC circuit with a higher capacitance. This would increase the time it takes for the ionization voltage to build up, thereby making it possible to distinguish different Rydberg states more easily and to be able to distinguish different angular momentum states from one another.

Nonetheless, it is possible to see that the time of flight of principal number 57 is slightly lower than that of principal numbers 54 and 55, which is what is expected according to theory.

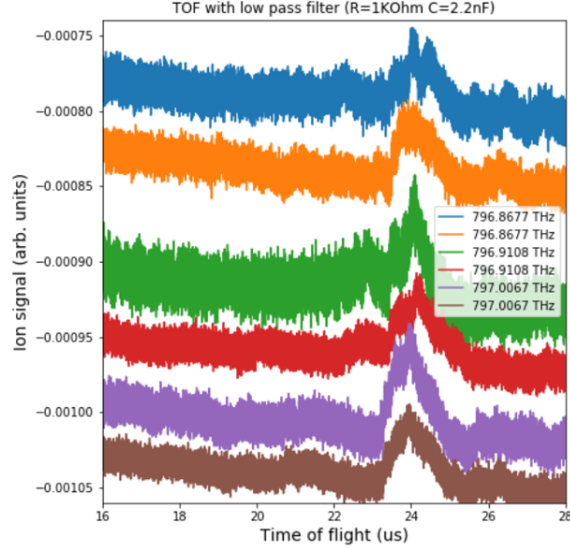


Figure 12: Time of Flight Measurements performed with a low pass filter ($R=1\text{k}\Omega$ and $C=2.2\text{nF}$) for Rydberg atoms with principal numbers 54 (blue and orange), 55 (green and red) and 57 (purple and brown)

4.5 Lifetime Measurements

In order to measure the lifetime of the different Rydberg states, one targets an individual Rydberg state by tuning the Rydberg excitation pulse to the transition frequency found in section 4.3.2. By setting the ionization pulse slightly above the ionization threshold (see section 4.1), one can measure the ion signal. However, instead of keeping the time delay τ between the Rydberg excitation pulse (375 nm laser) and the ionization field constant, one measures the number of detected Rydberg atoms as a function of time delay (14). By fitting the data with the exponential decay function $N(t) = N_0 e^{-t/\tau}$, it is possible to deduct the lifetime of different Rydberg states (15).

This can be shown in figure 13, where the lifetime of three different states was measured. By looking at the theoretical calculation of lifetimes for different states as shown in section A.2, it can be seen that higher Rydberg states are expected to have higher lifetimes. This is confirmed by the experimental data showing an average lifetime of $28 \pm 3 \mu\text{s}$ for the 50^1D_2 state, $34 \pm 5 \mu\text{s}$ for the 55^1D_2 state and $50 \pm 5 \mu\text{s}$ for the 60^1D_2 state.

Since blackbody radiation causes Rydberg states of higher principal number to unintentionally be measured in addition to the targeted Rydberg states, it is recommended to measure the time evolution slightly below the ionization threshold as well and subtract these values. This ensures that only the lifetime of a specific state is being measured (14).

This technique for measuring lifetimes of states can later be used to measure the lifetimes of circular Rydberg states.

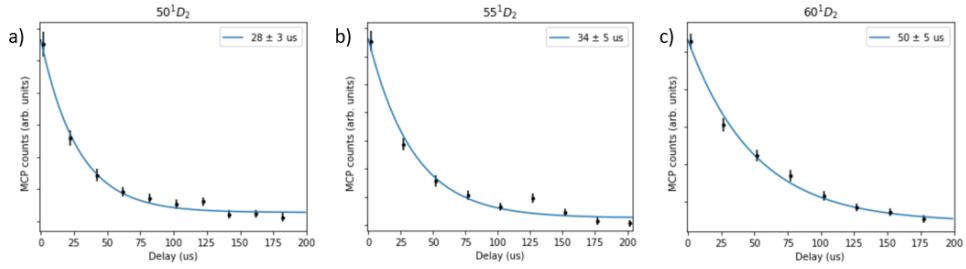


Figure 13: Lifetime measurements for states with principal numbers 50, 55 and 60 as calculated from the exponential decay fitting the MCP count data for various time delays τ

5 Conclusion and Outlook

In conclusion, pulsed field ionization in combination with Rydberg state detection using an MCP has made it possible to accurately detect specific Mg Rydberg states and thereby perform spectroscopy. This makes it possible to directly measure Rydberg atoms by ionizing them, instead of indirectly through loss of fluorescence as shown in figure 3. Using quantum defect theory (see section 4.3.1), it is then possible to assign these states to specific Rydberg states. This spectroscopy was performed for different states ranging from quantum number 54 to 117 (as can be seen in section 4.3.2).

Attempts to time-resolve different angular and magnetic quantum numbers l and m in time of flight measurements using time delayed field ionization (see section 4.4) were also performed. While it was possible to take time of flight measurements, no significant difference in time of flight for different states was yet detected, as seen in figure 12.

In order to better identify changes in time of flight, one approach is to include an RC circuit with a higher time constant $\tau = RC$. This would result in the voltage, which builds up in a $1 - e^{-t/\tau}$ fashion, to build up slower at voltages close to the final voltage. Although this leads to more ions being lost due to the general increase in time, this would lead to a better time resolution in order to distinguish time of flights for different states.

The lifetime of different Rydberg states were also measured, as can be seen in figure 13. The same experimental procedure to determine lifetime can also be used to measure the lifetime of circular Rydberg states.

In order to create the circular Rydberg states discussed above, it will be necessary to use a microwave source with frequencies at around 50 GHz. Since circular Rydberg states are states where the Rydberg electron is excited to a high quantum state with maximum angular momentum along the quantization axis, it is necessary to be able to resolve different l and m states (16).

6 Acknowledgements

Special thank you to Dr. Henry Fernandes Passagem for his kind guidance and support during this project. Without his help, this project would not have been possible.

I would also like to thank Prof. Dr. Jonathan Home for the opportunity to perform this semester thesis in his group. His course "Quantum Optics," as well as Dr. Daniel Kienzler's course "Trapped-Ion Physics" greatly sparked my interest in further pursuing research in this field.

Thank you to the entire Trapped Ion Quantum Information group for creating such a welcoming and collaborative environment.

List of Figures

1	Energy Level diagram for singlet states in Mg, depicting two-photon excitation to Rydberg states (not to scale).	5
2	Comparison of relative intensity of fluorescent Mg cloud (excited by 285 nm laser) and fluorescence drop due to Rydberg resonance	6
3	Loss in fluorescence due to resonant transition with 375 nm laser exciting a valence electron to Rydberg state as a function of frequency	6
4	Top view of the experimental setup showing the MOT and MCP chamber with a 285 nm and 375 nm laser (not to scale). A third beam coming from the 285 nm laser passes through the MOT from the top and cannot be seen in the image.	7
5	Simplified setup showing how 275 nm laser light is created using an infrared diode laser, a tapered amplifier (TA), multi-cavities containing LBO crystals, a beam splitter (BS) and laser locking using an iodine cell. Not to scale.	8
6	Side View inside the MOT, showing three mutually orthogonal, counter-propagating, polarized, red detuned 285 nm laser beams that enable trapping of neutral atoms. Modified figure from Kowalski et al. (7)	9
7	Anti-Helmholtz coils leading to a magnetic quadrupole field . . .	10
8	B field along the axis of two counter-propagating beams with opposite polarization, with the Zeeman shifted sublevels and Doppler shifted frequencies causing an atomic resonance transition shown below. Modified figure from Kowalski et al.	10
9	Time Sequence used for experiments, where the time delay τ is held constant (at $1.4 \mu\text{s}$) for the spectroscopy of Rydberg states and time of flight measurements. For lifetime measurements, one varies the time delay τ	11
10	Scanning the resonance frequency of the 375 nm laser for two different frequency ranges and measuring MCP count, finding the 54D and 55D states and their resonance frequencies	14
11	This graph shows a comparison between measured (solid lines) and calculated (dotted lines) resonance frequencies for two different frequency ranges	15
12	Time of Flight Measurements performed with a low pass filter ($R=1\text{k}\Omega$ and $C = 2.2\text{nF}$) for Rydberg atoms with principal numbers 54 (blue and orange), 55 (green and red) and 57 (purple and brown)	16
13	Lifetime measurements for states with principal numbers 50, 55 and 60 as calculated from the exponential decay fitting the MCP count data for various time delays τ	17

List of Tables

1	Quantum Defect Rydberg-Ritz Expansion Coefficients for Mg I (10)	12
2	Experimentally Measured Resonances	14
3	Calculated Transition Frequencies and Wavelengths	23

References

- [1] K. C. Young, “Rydberg atoms for quantum information,” phd thesis, University of Michigan, 2020.
- [2] T. F. Gallagher, *Rydberg Atoms*, ch. 1 Introduction, pp. 1–9. Cambridge University Press, 2005.
- [3] J. D. T. Sam R. Cohen, “Quantum computing with circular rydberg atoms,” *PRX Quantum* 2, vol. 030322, 2021.
- [4] E. G. W. S. E.J. Catanzaro, T.J. Murphy, “Absolute isotopic abundance ratios and atomic weight of magnesium,” *Applied Physics A*, vol. 70A, no. 6, 1966.
- [5] D. E. Kelleher and L. I. Podobedova, “Atomic transition probabilities of sodium and magnesium. a critical compilation,” *J. Phys. Chem. Ref Data*, vol. 37, 267, 2005.
- [6] T. Dressler, “Spectroscopy of high energy rydberg states of magnesium,” semester project, ETH Zürich, 2019.
- [7] K. D. X. M. G. B. N. H. J. S. K. Kowalski, V. Cao Long, “Magneto-optical trap: Fundamentals and realization,” *Computational Methods in Science and Technology*, vol. Special Issue 2, pp. 115–129, 2010.
- [8] T. F. Gallagher, *Rydberg Atoms*, ch. 6 Electric fields, pp. 70–101. Cambridge University Press, 2005.
- [9] T. F. Gallagher, *Rydberg Atoms*, ch. 20 Quantum defect theory, pp. 415–428. Cambridge University Press, 2005.
- [10] A. K. N. P. K. M. S.F. Dyubko, V.A. Efremov, “Laser-microwave spectroscopy of singlet mg i atoms in s,p,d,f,g rydberg state,” September 2013.
- [11] V. E. A. K. N. P. K.B. MacAdam, S.F. Dyubko, “Microwave spectroscopy of singlet mg i in l=0-4 rydberg states,” *Journal of Physics B: Atomic, Molecular and Optical Physics*, vol. 45, 2012.
- [12] L. S. Zhi M.C., Dai C.J. vol. 10, 2001.
- [13] J. R. Alexander Kramida, Yuri Ralchenko and N. A. Team, “Atomic spectra database.” ”<https://dx.doi.org/10.18434/T4W30F>”, October 2021.
- [14] Y. Z. X. H. Y.-y. L. Da-wei Fang, Wei-jun Xie, “Radiative lifetimes of rydberg state of ytterbium,” *Journal of Quantitative Spectroscopy Radiative Transfer*, vol. 69, 2000.
- [15] T. F. Gallagher, *Rydberg Atoms*, ch. 4 Oscillator strengths and lifetimes, pp. 38–49. Cambridge University Press, 2005.
- [16] P. G. S. H. J. Liang, M. Gross, “Circular rydberg-state spectroscopy,” *Physical Review A*, vol. 33, no. 6, 1986.

A Appendix

A.1 Calculated Transition Frequencies and Wavelengths

Table 3: Calculated Transition Frequencies and Wavelengths

State	Wavenumber [cm^{-1}]	Frequency [THz]	Wavelength [nm]
50S	26573.086177	796.641082	376.320610
50D	26574.799633	796.692450	376.296346
51S	26574.954925	796.697106	376.294147
51D	26576.567385	796.745446	376.271317
52S	26576.713708	796.749833	376.269245
52D	26578.232957	796.795379	376.247737
53S	26578.370985	796.799517	376.245783
53D	26579.804073	796.842480	376.225497
54S	26579.934422	796.846387	376.223652
54D	26581.287743	796.886959	376.204498
55S	26581.410970	796.890653	376.202754
55D	26582.690337	796.929008	376.184648
56S	26582.806951	796.932504	376.182997
56D	26584.017658	796.968800	376.165865
57S	26584.128122	796.972111	376.164302
57D	26585.274995	797.006494	376.148075
...
100S	26608.469926	797.701860	375.820182
100D	26608.677004	797.708068	375.817257
101S	26608.696300	797.708647	375.816984
101D	26608.897221	797.714670	375.814147
102S	26608.915947	797.715232	375.813882
102D	26609.110954	797.721078	375.811128
103S	26609.129133	797.721623	375.810871
103D	26609.318456	797.727299	375.808197
104S	26609.336109	797.727828	375.807948
104D	26609.519966	797.733340	375.805351
105S	26609.537113	797.733854	375.805109
105D	26609.715712	797.739208	375.802587

A.2 Lifetime of different Rydberg states

The main reasons for Rydberg state de-excitation are spontaneous emission, stimulated emission, as well as absorption due to blackbody radiation from the environment. The lifetime of an n state can therefore be written as follows:

$$\frac{1}{\tau_n} = \sum_{n' < n} A_{nn'} + \sum_{n' < n} B_{nn'} \rho_{nn'} + \int B \rho dE$$

the Einstein probability coefficient for spontaneous emission from state n to a lower state n' is given by $A_{nn'}$, while the Einstein probability coefficient for stimulated emission from n to n' is given by $B_{nn'}$. $\rho_{nn'}$ is the energy density of blackbody radiation.

$$A_{nn'} = \frac{4e^2 \omega_{nn'}^3}{3\hbar c^3} |r_{nn'}|^2 \quad B_{nn'} \rho_{nn'} = \frac{4e^2 \omega_{nn'}^3}{3\hbar c^3} \frac{|r_{nn'}|^2}{e^{\frac{\hbar \omega_{nn'}}{kT}} - 1}$$

$|r_{nn'}|$ is the dipole matrix element and $\omega_{nn'}$ is the transition frequency. By subtracting the population decay due to higher n states as described at the end of the experimental section 5.2, we can neglect contributions due to higher n states, leading to the following simplified expression:

$$\frac{1}{\tau_n} = \sum_{n' < n} (A_{nn'} + B_{nn'} \rho_{nn'}) = \sum_{n' < n} \frac{4e^2 \omega_{nn'}^3}{3\hbar c^3} = \sum_{n' < n} \frac{4e^2 \omega_{nn'}^3}{3\hbar c^3} \left[1 + \frac{1}{e^{\frac{\hbar \omega_{nn'}}{kT}} - 1} \right] |r_{nn'}|^2$$

Using Coulomb approximation one can now calculate the dipole matrix elements $|r_{nn'}|$. Using the energy level calculations in section 6.1 one can calculate the transition frequencies $\omega_{nn'}$. Combining these results with the equation given above makes it possible to find expected lifetimes for different Rydberg states (15; 14).